

submitted to AJ

The Stellar Populations of Spiral Disks. III. Constraining their evolutionary histories

Mercedes Mollá

Departamento de Física Teórica, Universidad Autónoma de Madrid, 28049 Cantoblanco, Spain

`mercedes.molla@uam.es`

Eduardo Hardy

National Radio Astronomy Observatory ¹

`ehardy@nrao.edu`

ABSTRACT

We study the old problem of the uniqueness of chemical evolution models by analyzing a set of multiphase models for the galaxy NGC 4303 computed for a variety of plausible physical input parameters.

We showed in Mollá et al. (1999) that multiphase chemical evolution models for the three Virgo cluster galaxies NGC 4303, NGC 4321 and NGC 4535, were able to reproduce the observed radial distributions of spectral indices Mg₂ ad Fe52. Chemical evolution models may, however, fit the present-epoch radial distributions with different star formation histories, thus we need to include time-dependent constraints to the problem. The two spectral indices above depend on the time-averaged history of star formation, but are in turn affected by the well known age-metallicity degeneracy which prevents the disentangling of age and metallicity for stellar populations, another uniqueness problem we also discuss.

Our aim is to determine if the possible input parameters may be strongly constrained when both radial distributions (nebular and stellar) are used. In order to accomplish this we run a large number of models (500) for NGC 4303 varying the model input parameters. Less than 4 % of the models (19) fit the present day observational data within a region of 95% probability. The number of models reduces to a ~ 1 % (6) when we also ask them to reproduce the time-averaged abundances represented by the spectral indices. Thus, by proving that only a small fraction of the models are favored in reproducing the present day radial abundance distributions and the spectral indices data simultaneously, we show that these spectral indices provide strong time-dependent additional constraints to the possible star formation and chemical histories of spiral disks.

Subject headings: galaxies: abundances – galaxies: evolution– galaxies: spiral – galaxies: stellar content

1. Introduction

Variations of abundances with galactocentric radius have been widely observed in external spiral galaxies (Díaz 1989; Skillman et al. 1996; Garnett et al. 1997), mostly via observations of H II regions which represent the abundances in the gas phase at the present time. Since Tinsley (1980), a large number of chemical evolution models have been developed, by including different physical mechanisms (see Götz & Köppen 1992; Köppen 1994) in order to reproduce these radial gradients.

In this work we use a multiphase chemical evolution model (MCEM) where an infall dependent on galactocentric distance and a two-step star formation law, whereby molecular clouds are formed before stars, are the basic hypotheses. The outcome is star formation simulating a power law in the gas density with an exponent $n > 1$. This model was first applied to the Solar Neighborhood (Ferrini et al. 1992), to the whole Galactic (MWG) disk (Ferrini et al. 1994, hereafter FMPD), and to the bulge (Mollá & Ferrini 1995). Next the same model was applied to disks (Mollá et al. 1996), and bulges (Mollá et al. 2000) of a set of spiral galaxies of different morphological types, the observed radial distributions of diffuse and molecular gas, oxygen abundances and star formation rate being successfully reproduced. It seems therefore that the MCEM produces results in good agreement with the data representing the present-day interstellar medium.

It is well known, from studies of the MWG, however, that by tuning in an appropriate way both the history of star formation and the infall rate it is possible to reproduce the same present-time radial distributions using very different evolutionary scenarios (see, for examples and further references, Mollá et al. 1992; Tosi 1996). Tosi (1988) early addressed this problem of the uniqueness of theoretical chemical evolution models. In fact, in most cases differences in this kind of models have no, or very small, effect on the observed radial distributions as was shown in Tosi (1996), where a comparison of models built by different groups was discussed. The only important characteristic that discriminates among the existing chemical evolution scenarios is the resulting *time evolution* of the radial gradients of abundances. This time evolution depends on the ratio SFR/Infall, which becomes the crucial quantity in determining whether abundance gradients steepen or flatten with time. If infall is the source of star-forming gas, the gradient flattens as the galaxy evolves and consumes this gas. Conversely, it steepens with the time if the effect of the infall gas is mostly that of diluting the metallicity. In other words, present time H II abundances are not sufficient by themselves to discriminate among the possible models of disk evolution. Since chemical abundance data other than those derived from H II regions are almost nonexistent for external galaxies, a check

¹The National Radio Astronomy Observatory is a facility of the National Science Foundation operated under cooperative agreement by Associated Universities, Inc., U.S.A.

on the time evolution of chemical models is only possible, in principle, for the MWG, where observational data for individual stars of different ages exist. This comparison was performed for the MCEM in Mollá et al. (1997)².

An independent test for the evolutionary history of external spiral disks as predicted by the chemical evolution models was proposed by Mollá et al. (1999, –hereafter Paper II). There we made use of the radial distributions of spectral indices Mg_2 and $Fe52$, obtained by Beauchamp & Hardy (1997), hereafter Paper I, and Beauchamp (1997) for three galaxies in the Virgo Cluster, NGC 4303, NGC 4321 and NGC 4535. The MCEM applied to these galaxies, reproduced the present radial distributions and also predicted, for the first time in spiral disks, the main characteristics of the radial distributions of Mg_2 and $Fe52$ indices. The reader must remember, as pointed out above, that the calibrated spectral indices represent abundance time-averages over the galaxy chemical history, as opposed to the accumulated effect shown by the extreme Pop. I objects such as H II regions or the B stars.

But even in the case under discussion we face an uniqueness problem because the spectral indices synthesis models also show a degeneracy in the plane Mg_2 - $Fe52$ (or $\langle Fe \rangle$) plane: Indeed, age produces almost the same effect as metallicity thus compromising their simultaneous determination for a given single stellar population, if only these two quantities are used (Barbuy 1994; Worthey 1994; Buzzoni et al. 1992, 1994). Other spectral indices, mostly those related to the Balmer lines, must be used in order to maximize the age-metallicity discrimination and to constraint the evolutionary parameters (Freitas-Pacheco 1998; Delisle 1998). The latter studies refer to elliptical galaxies where a high degree of coevality is assumed. Spiral disks are subject to a further difficulty in that stellar disks are composite systems and the time vagaries of star formation must be taken into account. They are on the other hand richer in information and physical constraints since data on the gas abundance and density are available and must be reproduced too.

Thus, there exists a possible ambiguity in that different star formation histories in disks are possible that would lead to the same final averaged spectral indices and/or present gas distributions. Are there alternatives to the SFR histories found in Paper II which may reproduce at the same time the present gas radial distributions and the stellar content information? Do both problems – uniqueness and degeneracy – go in the same or in opposite directions? In other words, can we constrain the possible sets of evolutionary histories on the basis of *all* the available observations?

In this work, we attack this problem by modifying the input parameters of the MCEM for the galaxy NGC 4303 for which we compute a large number (500) of different chemical evolution models. Then, by using a χ^2 optimization, we choose those able to fit the present-time nebular observations with probabilities larger than 97.5 %. Next, radial distributions of Mg_2 and $Fe5270$ are

²Another possible way to test the time evolution of the models is of course to calculate the evolution of abundances with redshift and to compare the predictions with the observations. This was successfully accomplished for damped Lyman alpha systems (Ferrini et al. 1997), but this procedure does not permit examining the time evolution of radial gradients, or the abundance variations in different regions of the same disk.

computed by using the chemical abundances and star formation histories predicted by the above-selected evolutionary models as input for the synthesis procedure employed to calculate spectral indices. We will determine if the comparison of these spectral indices distributions with the data helps in the final selection of the evolutionary histories valid over the disk.

In Section 2 we briefly describe the MCEM. The computed models as well as the method of selection among them, based on their predictions for the present epoch are also in Section 2. The calculation of synthesis models and the radial distributions of the spectral indices Mg₂ and Fe5270, as well as their comparison with observations, are shown in Section 3. We discuss these results in Section 4. Finally, our conclusions are presented in Section 5.

2. The Multiphase Chemical Evolution Model (MCEM)

2.1. A Brief Description

We remind the reader that the appropriate check of validity of the basic multiphase model, here adopted, has already been done in previous work, leaving open however the issue of uniqueness. Therefore, we only summarize here the MCEM whose detailed properties, as applied to spiral disks, are described in Ferrini et al. (1992, 1994); Mollá et al. (1996) and in Paper II of this series, and concentrate on the comparison among models.

In the MCEM a protogalaxy is assumed to be a spheroid composed of primordial gas with total mass $M(R)$. For NGC 4303 the latter is calculated from the rotation curves obtained either via radio (Guhathakurta et al. 1988) or optical (Distefano et al. 1990) observations. The galaxy is divided into concentric cylindrical regions 1 kpc wide. The model calculates the time evolution of the halo and disk components belonging to each cylindrical region. The halo gas falls into the galactic plane to form the disk, which in the multiphase framework is a secondary structure formed by the gravitational accumulation of the diffuse gas, g_H , at a rate f . The infall rate f is inversely proportional to the collapse time scale τ_{coll} , which is assumed to be dependent on galactocentric radius through an exponential function with a scale length λ_D :

$$\tau_{coll}(R) = \tau_0 e^{-(R-R_0)/\lambda_D} \quad (1)$$

The characteristic time scale τ_0 above is defined for every galaxy as being that of a region located at a radius R_0 , equivalent to the Solar Neighborhood (hereafter SN) in the MWG, which is itself scaled from $R_{\text{eff}} = 62.6$ arcsec (Henry (1992)). Thus, the adopted radius R_0 for this galaxy is 6 kpc. The value for the characteristic time scale may be determined, using the total mass of the galaxy, through the expression:

$$\tau_0 \propto M_9^{-1/2} T \quad (2)$$

from Gallagher et al. (1984), where M_9 is the total mass of the galaxy in $10^9 M_\odot$ and T is its age, assumed 13 Gyr. Thus, we obtain τ_0 for each galaxy, via the ratio:

$$\tau_0 = \tau_\odot (M_9, gal / M_{9,MWG})^{-1/2} \quad (3)$$

where $M_{9,MWG}$ is the total mass of MWG and the value of $\tau_\odot = 4$ Gyr, corresponding to the Solar Neighborhood, was determined in Ferrini et al. (1992).

In the various regions of the galaxy (halo or disk) we allow for the different phases of matter aggregation: diffuse gas (g), clouds (c , only in the disk), low-mass ($s_1, m < 4M_\odot$) and massive stars ($s_2, m \geq 4M_\odot$), and remnants. The mass in the different phases changes through several conversion process, all of them related to the rate of the corresponding star formation process:

1. Star formation by the gas spontaneous fragmentation in the halo ($\propto K g_H^{1.5}$)
2. Cloud formation in the disk from diffuse gas ($\propto \mu g^{1.5}$)
3. Star formation in the disk from cloud-cloud collisions ($\propto H c^2$)
4. Induced star formation via massive star-cloud interactions ($\propto a c s_2$)
5. Diffuse gas restitution from these processes

The rates for these processes are proportional to the parameters K , μ , H , and a , which, in turn, depend on galactocentric radius through the equations derived in FMPD. The proportionality factors in these equations are the corresponding efficiencies of the various processes, that is the efficiency of the halo star formation, ϵ_K , and, in the disk, the probability of cloud formation, ϵ_μ , of cloud—cloud collision, ϵ_H , and of the interaction of massive stars with clouds, ϵ_a .

The term ϵ_K is assumed constant for all halos, thus being independent of morphological type. The last term in the list above, containing the induced star formation, is associated to local processes and, as a result, its coefficient ϵ_a is considered independent of both position and morphological type. However, the other two rates, ϵ_μ and ϵ_H , depend on the Hubble type and/or the arm class. Therefore they must be chosen for each galaxy, their variation range being determined following the arguments given by Ferrini & Galli (1988), as discussed in Mollá et al. (1996) and in Paper II. These efficiencies resulted larger for earlier morphological types and lower for the later ones, and this is useful for the selection of initial values for a given galaxy as we showed in Paper II. Within this range, a fine tuning selection for these efficiencies ϵ_μ and ϵ_H is performed by choosing those for which the present time radial distributions (those of oxygen abundances, star formation rate, and the atomic and molecular gas surface densities) are well reproduced. We must stress that although each galaxy has its own set of efficiencies, the corresponding parameters μ , H , and K vary along the galactocentric radius.

The adopted initial mass function (IMF) is taken from Ferrini et al. (1990). The enriched material is the result of the restitution of processed material by dying stars and depends on their nucleosynthesis processes, their IMF (and delayed restitution) and their final fate, either via quiet evolution or via Type I or II supernova (SN) explosions. Nucleosynthesis yields used here are from Renzini & Voli (1981), for low and intermediate mass stars, and from Woosley & Weaver (1995) for massive stars, respectively. The type I supernova explosions release mostly iron, following Nomoto et al. (1984) and Brach et al. (1986), at a slower rate than type II, with the result that the iron appears at least 1 Gyr later than the α -elements (Oxygen, Magnesium ...) ejected by the massive stars.

The initial conditions are such that when star formation begins early in the halo zone and later in the disk (a secondary structure in our model), most of the barionic galactic mass has already accumulated. Boundary conditions are arbitrarily chosen: the first and simplest choice is to consider galaxies as closed systems. This choice does not strongly constraints the internally-driven phenomena – SN winds for example are not as prevalent during spiral galaxies evolution as to produce significant out-gassing, although they can influence internal redistributions. The environment in which galaxies live may have a sensibly larger importance (Henry 1993, 1996; Pilyugin & Ferrini 1998). We discuss here only *closed models*, keeping in mind that this is a first order approximation.

In the same spirit, we do not include at present in our models the effect of bars. It is quite evident, even from elementary dynamical considerations, that barred galaxies must present flatter radial gradients, as it has indeed been observed (Edmunds & Roy 1993; Martin & Roy 1992, 1994, 1995). We will simply consider that an eventual bar will influence the radial distributions only in the few internal kpc.

Summarizing, we will retain the same basic scenario applied to other spirals models but will vary the model input parameters, namely: *the characteristics collapse time scale*, τ_0 , according to the total mass, and the two efficiencies, ϵ_μ and ϵ_H , depending on the morphological type. The combination of selected parameters will therefore be different for each galaxy.

2.2. The Computed Models

Following the arguments above we had estimated in Paper II a value ~ 8 Gyr as the characteristics collapse time scale and a scale length λ_D of 4 kpc, for the galaxy NGC 4303. After estimating these parameters defining the collapse law, we chose the efficiencies ϵ_μ and ϵ_H , (0.22, 0.01), as those able to reproduce the observed radial distributions for the atomic gas (H I, Warmels 1988; Cayatte et al. 1990), the molecular gas (H₂, Kenney & Young 1988, 1989), the star formation rate surface densities obtained from H α fluxes from Kennicutt (1989), and finally the gas oxygen abundances (Henry 1992; McCall et al. 1985; Shields et al. 1991). In the present work will use the oxygen abundances as were corrected by Pilyugin (2000), which seem more adequate.

We proceed now to change the input parameters in order to take into account the uncertainties in the selection of that first set. Thus, for instance, the total mass depends on the maximum rotation velocity which, in some cases is different when calculated either from radio HI or optical data. For example, for NGC 4303, $V_{max} = 150$ km/s increases to a value around 216 km/s, from the first to the second data set. This factor of ~ 1.5 in velocity would translate into a factor of ~ 2.25 in τ_0 . Therefore, we must increase or decrease the collapse time scale by running models with 5 possible values for the characteristics collapse time scale: $\tau = 1, 4, 8, 12$ and 16 Gyr.

The relation between collapse time scale and mass makes it evident that τ_{coll} must change with galactocentric radius. If the total mass surface density follows an exponential form such as the surface brightness of spiral disks does, then the resulting τ_{coll} must increase along the radius with a scale length $\lambda_D \propto Re$ (where Re is the scale-length for the surface brightness distribution). This Re varies with the wavelength band and, moreover, it usually decreases for later types of galaxies and is larger for the earlier ones. Therefore, although we have so far used in our standard models $\lambda_D = 4$ kpc for all spiral disks, we must keep in mind the possibility of variations of this parameter. Thus, we take other 5 possible values for this scale length: $\lambda_D = 1, 4, 8, 12$ and 16 kpc.

The effects of changing efficiencies or the collapse time scale are not equivalent: by increasing the cloud and star formation efficiencies it is easier to form molecular clouds and also to destroy them to produce stars, thus resulting in a star formation rate with higher absolute values, but maintaining the same star formation history. In other words, the maximum of the star formation rate will occur always at the same time for models with the same τ_{coll} . Alternatively, a longer collapse time scale means a lower infall rate on the disk, resulting into a star formation rate which shifts its maximum to a later time, producing therefore a slower evolution even with the same absolute value of its maximum. From Eq.1 the scale length λ_D , changes the rate of evolution among different radial regions, increasing the differences among them if it is small or decreasing them when it is large, thus acting upon the radial gradients of abundances, which become steeper (or flatter) when the parameter λ_D is shorter (or larger).

In order to check the effect of the degeneracy problem in the plane $Mg_2 - Fe52$, it is crucial to analyze the differences among the ages of stellar populations predicted by models with varying collapse times or length scales, and their effects on spectral indices.

Efficiency values and collapse times are constrained variables that change together. These probabilistic efficiencies may take values from 0 up 1, and we assume that they depend on the morphological type, following the equations:

$$\epsilon_\mu = e^{-T^2/15} \quad (4)$$

and

$$\epsilon_H = e^{-T^2/5} \quad (5)$$

where T is the Hubble type (see Mollá et al. 2002), which gives values similar to those from Paper II where $T = 4$, the morphological type assigned to NGC 4303.

Because these values might change if we vary the infall rate law, we have also run models with 20 possible values for each set $(\epsilon_\mu, \epsilon_H)$, calculated from the above expressions, simulating 20 different morphological types from 0 to 10 (by including intermediate values as 0.5, 1.5, etc...). Thus, we ran a total of 500 models, with all possible variations of these three parameters, τ_0 , λ_D and the set $(\epsilon_\mu, \epsilon_H)$ –or equivalently the value of T –.

2.3. The most probable models from the present day observations

We must now select which set of parameters among these 500 models are adequate to represent the observed present-time radial distributions of abundances, star formation rate, and diffuse and molecular gas density.

In order to do that, and following the technique used by Tosi (1988) in her uniqueness problem study, we compute the χ^2 indicator, which measures the proximity of a model to the region limited by observational error bars:

$$\chi^2 = \sum_{i=2}^{14} \frac{(Y_{cal,i} - Y_{obs,i})^2}{\sigma_i^2} \quad (6)$$

where $Y_{cal,i}$ is the computed quantity, in each radial region i , $Y_{obs,i}$ is the corresponding observed quantity at the same galactocentric distance, and σ_i is the error in quantity.

We compute our models for radius from 2 up to 14 kpc in steps of 1 kpc, by avoiding the inner region or bulge because it has a different geometry and structure. Therefore, i takes values from 2 to 14. The value σ_i is taken as ~ 0.2 dex for the oxygen abundances, the current error in the estimates of abundances, and $\sim 2M_\odot/\text{pc}^2$ for the HI surface density, a mean value estimated for these types of data. For the star formation rate and the molecular cloud surface density we assume errors as larger as 40% and 50%, respectively, due to the larger uncertainties involved in the derivation via H α and CO fluxes. In particular, we must take into account that the H $_2$ masses in a given region are estimated through a scaling factor α which depends on the metallicity of this region (Verter & Hodge 1995; Wilson 1995). Due to the uncertainties involved in the calculation of this parameter, the corresponding radial distribution of $\sigma(\text{H}_2)$ are considered doubtful (Taylor & Klein 2001).

After computing the χ^2 indicator for each radial distribution of oxygen, star formation and gas surface densities produced by our 500 models we must choose the possible models or the range in the input parameter which may produce models with results falling within the confidence region. In order to do that, we first select the model corresponding to the lowest values of χ^2 , χ^2_{min} , for each set of observations, that is the maximum-probability model for each constraint.

We now select those models for which $\chi^2 - \chi^2_{min} < A$, A being the selected value for a given probability which takes into account the free parameters of the sample and selects the confidence region for the parameter set. From the number of radial regions, parameters and observational constraints, we search for the parameter region with $\chi^2 - \chi^2_{min} < 5.62$, that is probabilities larger than 97.5% for each individual data set or larger than 90% for all of them over the region of superposition. In this way, for each model and observational constraint, we have a value of χ^2 , and its corresponding probability P .

In order to choose the best models, we must obtain the region of parameters that minimize their χ^2 for each radial distribution of data separately, and then find the region of coincidence. Accordingly, we represent these regions of high probabilities for each observational constraint, all on the same figure so as to delimit the values of the most probable input parameters. When there are two free parameters in the theoretical model finding the plane *parameter1-parameter2* for which each set of constraints has a large probability of being well fitted, is relatively easy. In practice we are dealing with a 3 parameters space— τ_0 , λ_D and the set (ϵ_μ and ϵ_H), or its equivalent T value. Thus, in order to find the region of parameters that reproduce *all* observations with a high probability we will rely on projections of these planes taking two parameters at a time.

In fig. 1, (panels a to e), we show the probability contours for each radial distribution plotted, as function of type T and of the collapse time scale τ_0 (in Gyr). These 5 panels, one for each λ_D value, are the successive projections on the plane $T - \tau_0$ of our 3-dimensional regions along the λ_D axis. Those parameters which give probabilities larger than 97.5% for the oxygen abundance $12 + \log(O/H)$ ($P_{OH} > 0.975$) are represented by solid lines. The dotted lines represent the star formation rate surface density ($P_{SFR} > 0.975$) and the atomic and molecular surface densities ($P_{HI} > 0.975$ and $P_{H_2} > 0.975$), are represented by the long and short dashed lines. The shaded regions are the coincidence regions where all constraints are reproduced simultaneously with $P > 90\%$.

In panel a) there are no successful models, all of them produce probabilities smaller than 97.5% of fitting the observational data. It is therefore clear than $\lambda \geq 4$ kpc. The panel with the largest number of acceptable possibilities correspond to $\lambda = 8$ kpc where the region of coincidence is the largest of the five. The longer the collapse time scale the larger must be the scale length. In effect, if $\lambda_D = 4$ kpc, $4 < \tau_0 < 12$ Gyr; if $\lambda_D = 8$ kpc $\tau_0 > 8$ Gyr, while if $\lambda_D = 12$ or 16 kpc, $\tau \geq 10 - 12$ Gyr. For all these possibilities, efficiencies fall within a very limited region of $4 \leq T \leq 5$.

The latter statement is also apparent from panels f) to j), where the same kind of probability contours are shown for the plane $T - \lambda_D$. From them, we can eliminate the shortest collapse time scale ($\tau = 1$): only if $\tau > 4$ Gyr it is possible to have coincidence at a level larger than 90 % for all data. If $\tau = 4$ Gyr, only a value of $\lambda_D = 4$ kpc is possible. If $\tau = 8$ Gyr, then $4 \geq \lambda_D \geq 8$ kpc. Only for larger collapse time scales, larger values of λ_D , up to 16 kpc, are also possible.

From the graphs above, it is evident that only efficiencies corresponding to a T between 4 to 5 (i.e., only intermediate and late Spirals) are possible. Selection of other efficiency values would

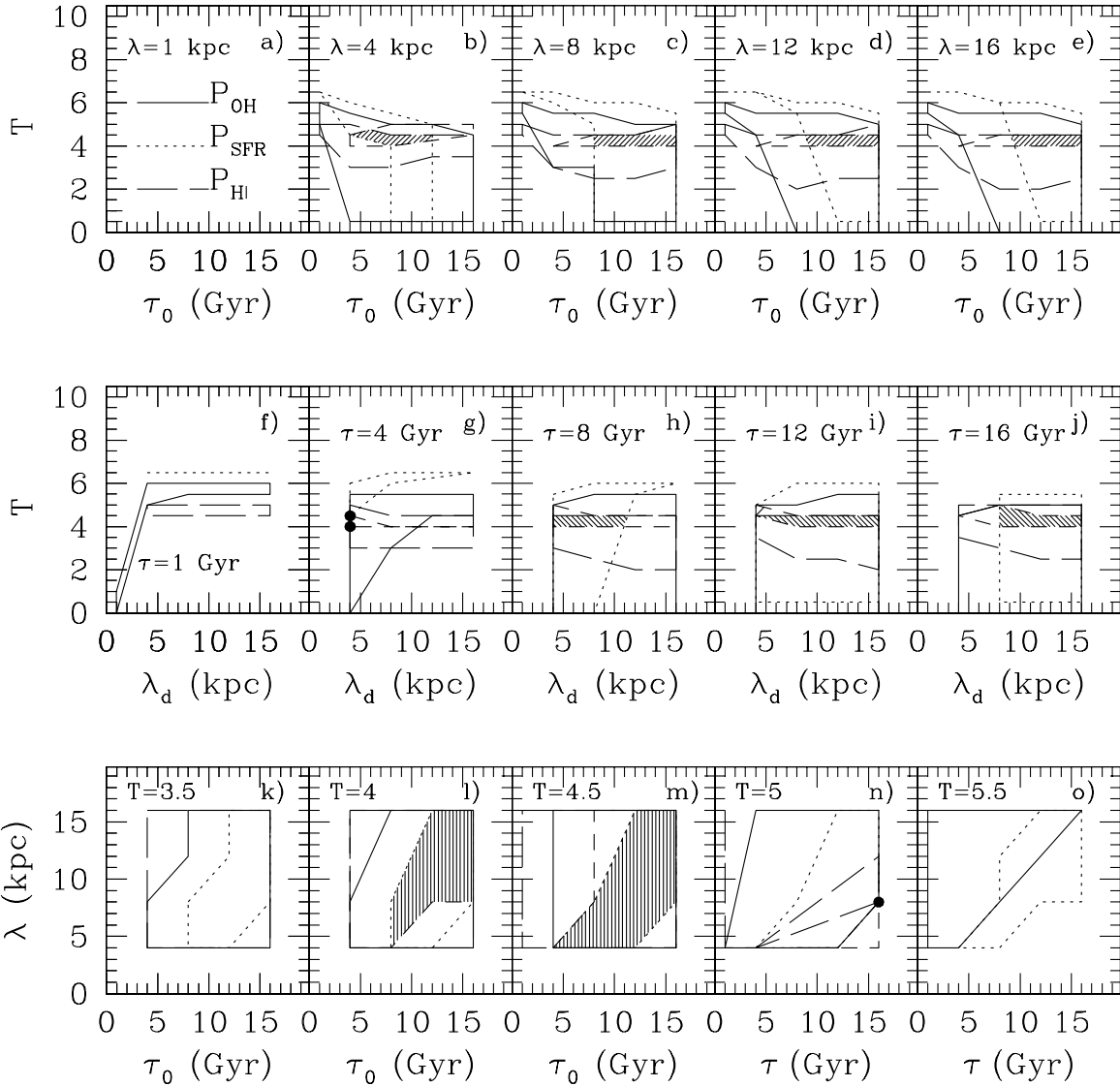


Fig. 1.— Probability contours representing regions where $P > 97.5\%$, for each observational constraint. Top panels, from a) to e), as a function of T and τ_0 . Central panels, from f) to j), as a function of T and λ_d . Bottom panels, from l) to o), as a function of τ_0 , and λ_d . The solid line represents the contours for the oxygen abundances. The same for the star formation rate surface density are the dotted lines, and for the atomic and molecular gas surface densities are the long-dashed and the short-dashed lines, respectively. The shaded regions (or the full dots when there is no region) are the zones of coincidence of these 4 contours, showing the range of parameters more probable than 90%.

produce poor fittings, mostly in the gas radial distributions, –long and dashed lines–, for which χ^2 increases abruptly if $T < 4$ or $T > 5$. The bottom panels from k) to o), represent the plane $\tau_{col} - \lambda$ for T values from 3.5 to 5.5. For values out of this range, there are again no coincidence regions. It is also clear from these panels that $\tau_0 \geq 4 - 8$ Gyr, and $\lambda_D \geq 4$ kpc are limiting values to obtain good models. Furthermore, it is also evident that the efficiencies values are strongly constrained by the gas densities, and that the use of both the diffuse and molecular gas densities, instead of the total gas mass or the gas fraction, proves superior in finding models fitting the present– day data.

The allowed morphological types reduce only to 2 possible values, $T = 4$ or $T = 4.5$, in excellent agreement with the type $T = 4$ given for NGC 4303. If $T = 5$ only a model (with $\tau = 16$ Gyr and $\lambda_D = 8$ kpc, is able to fit all constraints. Other T values, or different efficiencies of diffuse gas and molecular cloud formation have null probabilities of fitting the gas radial distributions. Since the morphological type is at least partially defined by the amount of gas on the disk we do not regard this as a surprising result, but are reassured that our efficiencies for the different morphological types are well chosen.

To summarize, the present method yields parameters for which the model results are within the region defined by the error bars with a confidence level A. We reduce our possibilities to a λ_D larger than 4 kpc, a characteristic collapse time scale between 4 and 16 Gyr, and efficiencies corresponding to morphological types $T = 4$ or 4.5 . Only 19 models out of 500 satisfy these conditions, thus reducing the possible chemical evolution models to a $\sim 4\%$ of the initial number.

We show in Table 1 χ^2 and the corresponding probability P for each one of the observational constraints, for these 19 models which have probabilities larger than 97.5% to be close to the observations (which in turn corresponds to 90% for the combination). There we have in column (1) the number identifying our model. Column (2) is the value of T. The characteristics collapse time scale, τ_0 , and the scale length, λ_D , are in columns (3), and (4). Efficiencies ϵ_μ and ϵ_H are given in columns (5) and (6). In Columns (7) to (10) the values of χ^2 , corresponding to the radial distributions of abundances, star formation rate, and diffuse and molecular gas surface densities, are given. Finally, the probabilities of these distributions to be in a region around the minimum value of χ^2 are in columns (11) to (14). We conclude there is only a model with $\tau_0 = 4$ Gyr and only a model with $T = 5$. All the others correspond to $T = 4$ or 4.5 with $\tau_0 \geq 8$ Gyr.

2.4. Present Day Radial Distributions

Following the procedure described above we have found 19 different models for N4303 satisfying the condition that the radial distributions of abundances, star formation rate and gas densities all have probabilities larger than 90% of fitting the observational data.

We represent all models in Fig. 2 where we see that all of them are falling within the regions defined by the observational limits, obtained with the data and the error bars and represented by the thick solid lines. We regard the latter subset of models as equally probable within the errors

Table 1. Parameters of the Selected Models ($P > 90\%$)

Model	T	τ	λ_D	ϵ_μ	ϵ_H	χ^2_{OH}	χ^2_{SFR}	$\chi^2_{\text{H}_1}$	$\chi^2_{\text{H}_2}$	P_{OH}	P_{SFR}	P_{H_1}	P_{H_2}
129	4.	4.	4.5	.259	.017	0.957	6.040	0.378	2.318	1.000	0.983	1.000	1.000
228	8.	4.	4.0	.344	.041	1.201	2.114	1.401	6.413	1.000	1.000	1.000	0.983
229	8.	4.	4.5	.259	.017	0.361	1.716	1.670	1.672	1.000	1.000	1.000	1.000
248	8.	8.	4.0	.344	.041	3.416	5.335	0.265	4.814	0.999	0.992	1.000	0.998
249	8.	8.	4.5	.259	.017	1.922	5.119	1.681	3.177	1.000	0.993	1.000	1.000
329	12.	4.	4.5	.259	.017	0.714	4.887	2.690	2.806	1.000	0.995	1.000	1.000
348	12.	8.	4.0	.344	.041	2.647	2.896	0.689	5.276	1.000	1.000	1.000	0.995
349	12.	8.	4.5	.259	.017	1.223	2.533	1.352	2.101	1.000	1.000	1.000	1.000
368	12.	12.	4.0	.344	.041	3.398	4.783	0.435	4.985	0.999	0.996	1.000	0.997
369	12.	12.	4.5	.259	.017	1.937	4.505	1.562	3.238	1.000	0.997	1.000	1.000
388	12.	16.	4.0	.344	.041	3.773	6.222	0.402	4.947	0.998	0.980	1.000	0.997
389	12.	16.	4.5	.259	.017	2.336	6.089	1.799	4.032	1.000	0.982	1.000	0.999
448	16.	8.	4.0	.344	.041	2.095	3.567	1.337	6.075	1.000	0.999	1.000	0.988
449	16.	8.	4.5	.259	.017	0.858	3.219	1.130	2.056	1.000	1.000	1.000	1.000
450	16.	8.	5.0	.189	.007	1.506	2.976	5.057	3.874	1.000	1.000	0.989	1.000
468	16.	12.	4.0	.344	.041	2.841	3.930	0.804	5.543	1.000	0.999	1.000	0.993
469	16.	12.	4.5	.259	.017	1.440	3.480	0.918	2.611	1.000	1.000	1.000	1.000
488	16.	16.	4.0	.344	.041	3.215	4.675	0.634	5.387	0.999	0.996	1.000	0.994
489	16.	16.	4.5	.259	.017	1.795	4.237	0.965	3.167	1.000	0.998	1.000	1.000

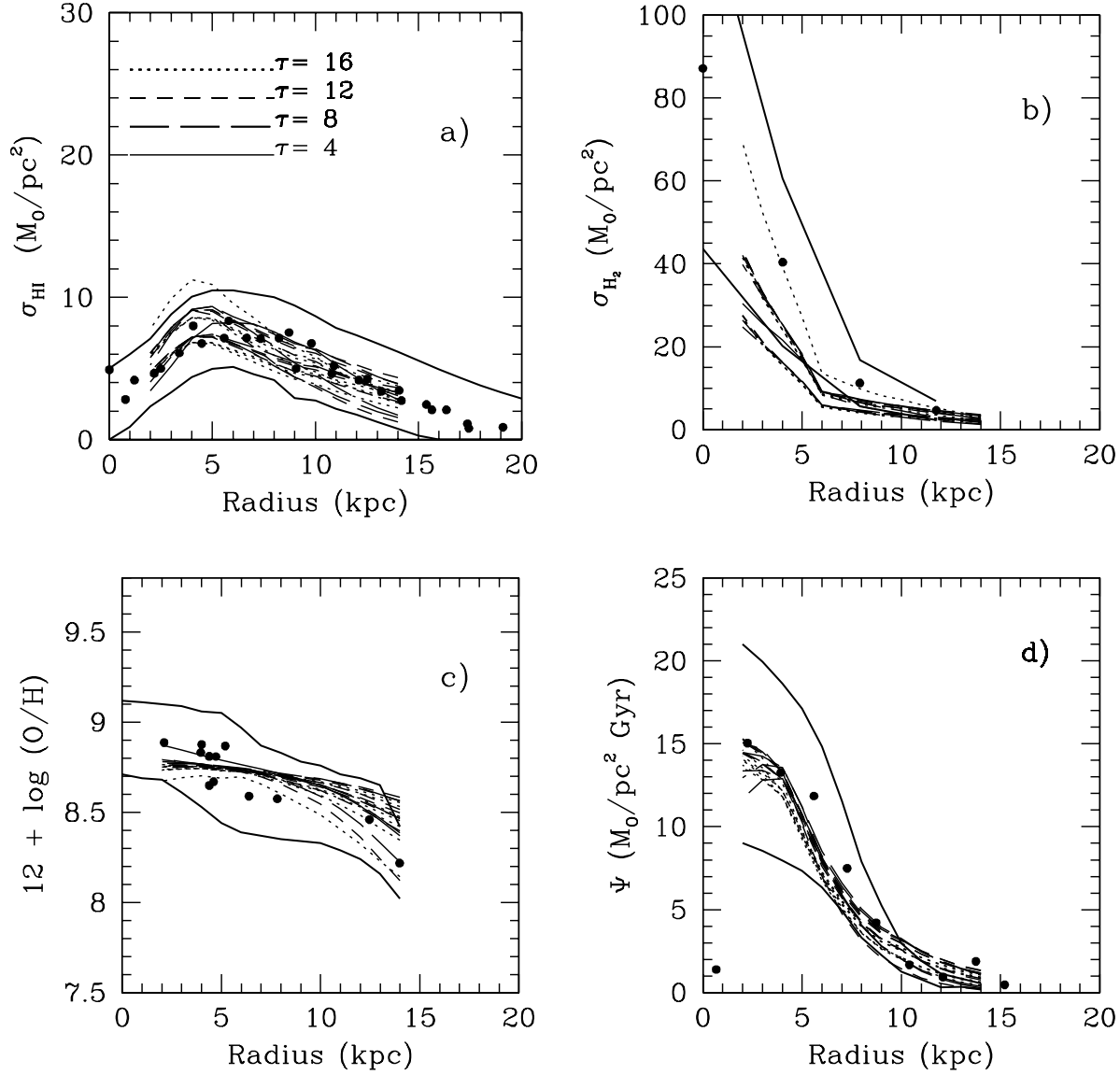


Fig. 2.— Predicted Radial distributions for models which satisfies the condition $P > 90\%$ simultaneously for all present time data: a) diffuse or atomic gas $\text{H}\alpha$ surface density; b) molecular gas H_2 surface density; c) Oxygen abundance as $12 + \log(\text{O}/\text{H})$ and d) Star Formation Rate surface density. Models are represented by different lines and symbols following the figure. Observational data are the full dots while the thick lines limit the region within observational error bars used in our realizations.

and seek now additional constraints to isolate the best models among them, representing the true evolutionary history of the galaxy.

3. Using Evolutionary Synthesis Models

Unlike HII abundances, whose abundances reproduce the cumulative effect of all past generations of stars, stellar indices contain information on the evolutionary history of a galaxy in the form of an average over time and over the SFR. They provide therefore additional constraints to our models and we show in this section how to retrieve this information.

3.1. The method of calculation

As pointed out, for N4303 (and two other galaxies of paper II) in addition to the typical quantities necessary to define the galactic evolution (i.e., gas, metals,...), we have at our disposal measurements of radial distributions of the spectral indices Mg_2 and $Fe52$. The fact that the models selected in the preceding sections represent well the present-day radial distributions, does not imply that the evolutionary history given by the multiphase model are unique, as no time-dependent information has been used so far. In fact, we have obtained results in agreement with the present gas data either with fast evolution (such as Model 129 with $\tau_0 = 4$ Gyr) thus producing stellar populations biased toward older ages and an earlier enrichment, or with a slower creation of stars (such as Model 450 $\tau_0 = 16$ Gyr) thus producing metals at a more constant rate. Both alternatives yield almost the same present radial distributions. Would they also produce similar radial distribution of stellar spectral indices? We will now compute these indices for each of our models in an attempt to answer this question, and will try to check if the radial distribution of spectral indices are equally well reproduced by the adopted set of models.

We proceed in a self-consistent way as follows. Using the chemical evolution models already described we calculate the integrated mass of stars created in a given time interval by the gas, and the mean abundance reached at that epoch by the same gas. We consider the resulting stellar populations residing in every galactocentric region as the superposition of a set of single stellar populations or *generations*, each one of which is defined by its age and its metallicity. We remind the reader that our models provide abundances for 15 elements, including Oxygen, Magnesium and Iron, so we know in addition the abundance ratio $[Mg/Fe]$ for each generation. We have in principle the necessary ingredients to evaluate observable spectral indices via a synthesis model.

Spectral index features are calculated with the same method described in (Mollá & García-Vargas 2000) by using the Padova group isochrones. The technique in question was developed to be used specifically in spiral disks or in regions where a combination of stellar populations of different ages and/or metallicities is necessary, and it works by simultaneously computing the spectral features and the continuum flux. An isochrone is assigned to each of our stellar generations

using the total abundance Z reached at this time step and the corresponding age. Then, an index value is calculated for each star belonging to that generation following its stellar gravity $\log g$, effective temperature T_{eff} and metallicity or abundance, through the fitting functions, and a synthetic spectra from atmosphere models is selected. By adding all stellar contributions, the contribution of every generation to both synthetic single continuum and line fluxes is computed at the same time. Next, continuum and line fluxes are added for all generations, weighted by the stellar mass created in every time step, according to the star formation history provided by the evolution model. This calculation is performed for all disk regions, generating spectral indices along the galaxy disk.

We use the fitting function from Worthey et al. (1994) for assign the index Fe52 to each star. However, the fitting function for Mg_2 must depend on the abundance $[\text{Mg}/\text{H}]$, not $[\text{Fe}/\text{H}]$, contrary to what is assumed in that work. The selection of $[\text{Mg}/\text{H}]$ or $[\text{Fe}/\text{H}]$ in spiral disks is important due the different rate in the ejection of these elements and the differences among the disk regions along the radius. Alternatively, Borges et al. (1995) obtained a fitting function for the index Mg_2 by including a dependence on $[\text{Mg}/\text{H}]$. However this dependence is derived from the relative abundance $[\text{Mg}/\text{Fe}]$. We prefer to use directly the dependence on $[\text{Mg}/\text{H}]$. Therefore, by using the same the stellar library from these authors, we have derived our own fitting function which gives us the direct dependence of Mg_2 on $[\text{Mg}/\text{H}]$. The abundance of $[\text{Mg}/\text{H}]$ is used to calculate Mg_2 and the abundance of $[\text{Fe}/\text{H}]$ to calculate Fe52.

3.2. Spectral indices results

We have computed in this way the radial distributions of spectral indices for all models of the galaxy NGC 4303 with larger than 90% probability in all observational constraints for the present-time data, as displayed in Table 1.

Can the comparison with spectral index radial distributions help us further in selecting the best evolutionary model or models, or limit the range of parameters of these?.

We compute once again the statistical indicator χ^2 but this time for each one of the two distributions as given by spectral indices. The results of these calculations are shown in Table 2, where we give the goodness of fit for each model. For each model number given in Column (1), Column (2) gives χ^2 for the Mg_2 data, Column (3) for Fe52. The corresponding probabilities are in Columns (4) and (5). The radial gradients obtained for each model and by the observational data distributions are also given in Columns (6),(7) and (8).

In Fig.3 we represent the same panels l) and m) from Fig. 1 but limiting those resulting regions with these new constraints. In panel a), $T=4$, we see that there is only a point, this one corresponding to Model 129, which satisfies our confidence condition of 97.5% for all observational constraints. For panel b), $T=4.5$, there still exists a little region shaded by both vertical and horizontal lines (that one shaded only by vertical lines correspond to the region obtained with

Table 2. Results from synthesis models.

Model Number	$\chi^2_{\text{Mg}_2}$	χ^2_{Fe52}	P_{Mg_2}	P_{Fe52}	Radial Gradients		
					$\nabla_{\text{O/H}}$	∇_{Mg_2}	∇_{Fe52}
* 129	5.30	3.17	1.00	1.00	-0.079	-0.0062	-0.094
* 228	6.69	3.94	1.00	1.00	-0.076	-0.0048	-0.074
* 229	6.60	4.89	1.00	1.00	-0.086	-0.0050	-0.078
248	11.06	3.49	0.97	1.00	-0.050	-0.0030	-0.045
* 249	10.51	4.41	0.98	1.00	-0.059	-0.0037	-0.056
* 329	8.30	6.75	1.00	1.00	-0.091	-0.0048	-0.075
348	11.80	5.02	0.95	1.00	-0.055	-0.0031	-0.047
* 349	10.70	6.29	0.98	1.00	-0.063	-0.0035	-0.054
368	12.81	4.90	0.91	1.00	-0.047	-0.0023	-0.034
369	13.41	4.82	0.88	1.00	-0.054	-0.0021	-0.031
388	13.41	4.82	0.88	1.00	-0.043	-0.0021	-0.031
389	13.17	6.01	0.90	1.00	-0.050	-0.0028	-0.042
448	12.19	6.04	0.94	1.00	-0.058	-0.0030	-0.046
449	14.38	10.92	0.83	0.90	-0.066	-0.0037	-0.057
450	14.38	10.92	0.83	0.90	-0.072	-0.0037	-0.057
468	13.13	5.94	0.90	1.00	-0.050	-0.0025	-0.037
469	12.49	7.41	0.93	0.99	-0.057	-0.0030	-0.047
488	13.61	5.87	0.87	1.00	-0.046	-0.0023	-0.034
489	12.73	7.32	0.92	0.99	-0.053	-0.0029	-0.043
OBS					-0.078	-0.0086	-0.073

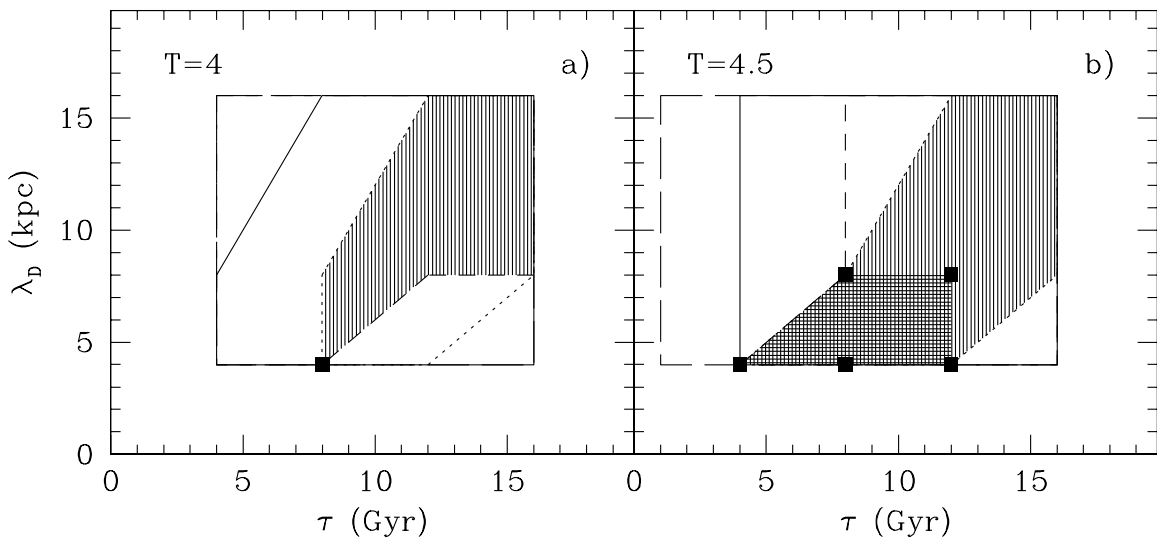


Fig. 3.— Probability contours representing regions with $P \geq 97.5\%$ for all observational constraints for $T = 4$ (panel a) and $T = 4.5$ (panel b) as a function of τ and λ . Lines represent the same than panels l) and n) from Fig. 1, while filled squares are the models obtained in Section 3.2

chemical evolution models) showing the possible input parameters which reproduce all data with the same goodness. There are more than one model, but we have restricted the possibilities to a very reduced zone.

The best model fitting the observational data with $P = 1$ for all constraints, corresponds to Model 229, with a morphological type $T = 4.5$, a collapse time scale $\tau_{\text{coll}} = 8$ Gyr and $\lambda_D = 4$ kpc, a model similar to Model B presented in Paper II as the best model. Only 5 other models, marked with an *, have also able to fit these new constraints with probabilities larger than 97.5%. In particular, Model 129, the only one among the 19 with $\tau_0 = 4$ kpc, have also high values of probabilities. All the other possible models, mostly in the low part of the table, that is with slow collapses and/or low star formation efficiencies, although reproduce the present day radial distributions, are far away from our confidence region for one or both spectral indices. Thus, Model 450, with $P \geq 0.99$ in Table 1 decreases its probabilities, when the comparison of model predictions with data is performed through the spectral indices Mg_2 and $\text{Fe}52$, to 0.83 and 0.90, respectively. Therefore, we reduce to 6 the possible models from the initial 500, this is only 1 % of them are retained by the procedure.

We may answer to the stated question, can the comparison with spectral index radial distributions help us to select the appropriate evolutionary model? with an affirmative statement. There are some sets of physically plausible input parameters that provide an adequate enough fit to the abundance data. However, these models can not reproduce equally well the spectral indices radial distributions.

We show in Fig. 4 the predicted radial distributions of Mg_2 (in panel a), and $\text{Fe}52$ (in panel b), respectively, for these 6 models. In the graphs of $\text{Fe}52$, observational points in the outer disks ($R > 10$ kpc) of all galaxies tend to increase with radius; we think that some of these points at large and moderate radii may be affected by large systematic uncertainties in the sky-subtraction procedure. The comparison of models with these $\text{Fe}52$ outer data is not significant.

For both indices there is an inner region where the observed values raise significantly. This region seems to contain a stellar bar which cannot be simulated with our present models, and as discussed, we have not included these regions in our calculations. However, we have added the results obtained for the bulge or central region with the Model B from Paper II in Mollá et al. (2000). The only difference between this bulge model and the disk models used here resides in the geometry and structure of this region. The input parameter for this bulge model are very similar to Model 229. Taking into account that the most of differences among models appears in the the outer disk predictions, we can assume that by using the 5 other model input parameters in the bulge model would give similar results for this bulge or central region. These results are shown in Fig.4 as open squares located in a mean radius for the bulge, assumed as 1 kpc. We have not computed the complete model with the full radial range included, for which a model allowing the calculation of radial gradients in the bulge is necessary. We believe that these central values fall on the right absolute level, and that the shape of the spectral indices distributions in the inner disk

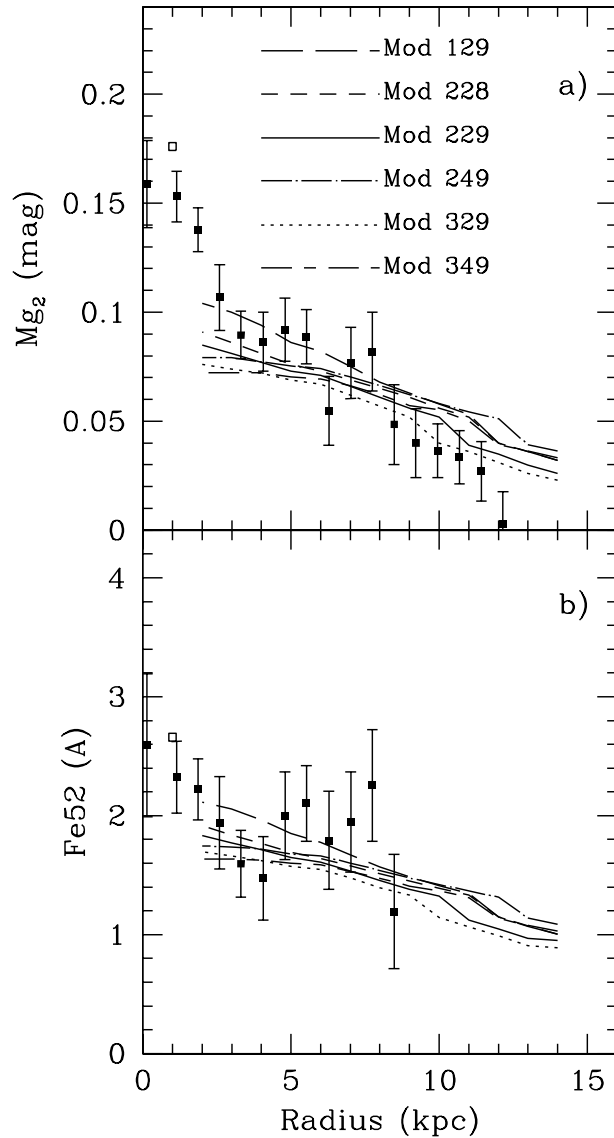


Fig. 4.— Spectral indices radial distributions for NGC 4303. Panel a) the index Mg₂ in magnitudes. Panel b) The index Fe₅₂ in Å. Data are from Beauchamp (1997) and Beauchamp & Hardy (1997).

may be also well reproduced.

Summarizing, the uniqueness issue associated the chemical evolution models is not strong, because the models were already reduced to a 5% with just the present day data as constraints. But when we use in addition the spectrophotometric indices we limit even more the possible evolutionary histories.

3.3. The origin of the radial variations of Magnesium and Iron

What is the explanation for the strong observed Mg2/Fe52 radial gradient? Indeed, computing the Mg2/Fe52 ratio from the data in columns 6,7 and 8 of Table 2 the gradient turns much more steeper in the observational data than predicted by the models. We have no straightforward explanation for this behavior.

From a chemical evolution point of view Magnesium appears early in the evolution, as it is produced by massive stars which evolve rapidly. Iron, instead, is created by the explosions of SN-I which need a time delay to appear. Although abundances tend to a saturation level, saturation is reached earlier for Magnesium, and as a result the Iron radial gradient subsists longer than the Magnesium one.

When stellar averaged abundances are computed, taking into account that star formation rate proceeds more rapidly in the inner disk than in the outer regions, an abundance flattening results which is very similar for both indices. In fact, the averaged stellar relative abundance $\langle [\text{Mg}/\text{Fe}] \rangle$ is almost zero for our 6 models, without appreciable variations along the disk.

We must remember, however, that spectral indices are not directly equivalent to abundances because they also depend on the mean age of the parent stellar populations. Therefore, one might think that the explanation for the strong radial gradient of the ratio Mg2/Fe52 could reside in the different dependence on age for both indices. It is well known in fact that Mg2 changes with age more strongly than Fe52. This dependence is however already included in the synthesis models through the fitting functions which include a component that varies with the effective temperature of stars. Thus, the models should be able to predict the observational data.

Maybe our models do not contain a sufficient variation in the mean age of the stellar populations along the radius. It is possible to obtain stronger radial gradients in age by decreasing the collapse time scale, for example $\tau_{\text{coll}} = 1$ Gyr, or by taking a shorter scale length λ_D . Both possibilities have been already included in our initial 500 models. But it should be noted that these types of models evolve very rapidly in the inner disk by swiftly consuming all the gas, even the molecular phase. The resulting radial distributions of molecular gas density show a hole in the center in clear disagreement with the observed exponential shape. It is also useful to remember that the uncertainties in the estimations of the molecular phase mass is large, due mostly to the dependence of its calibration on the metallicity of the region under study. We suspect that if this dependence

is included, the density of molecular gas in the inner disk could decrease and the models would change accordingly.

Other possible solution is that the age dependence of Mg2 or Fe52 included in the fitting functions is inadequate. The fitting function for Mg2 from Borges et al. (1995) has a stronger dependence on age than the one from Worthey (1994), but the parameters range for the first library is narrower than for the second one. The latter may produce problems when young populations coexists with the older ones, as is the case in spiral disks. This is particularly so in the outer regions, precisely where models differ more from the observations.

In our simple scenario the disk is created from the collapse of the gas of the protogalaxy. One might however think that other mechanism such as mergers are also able to produce variations in the ratio of Magnesium to Iron. Existing models for elliptical galaxies seem to indicate that in the merger scenario a ratio $[\text{Mg}/\text{Fe}] > 0$, and larger in the center, cannot be obtained (Thomas 2000). In fact the observed trends in $[\text{Mg}/\text{Fe}]$ are the opposite to those derived from the semianalytical models simulating mergers of spiral to form ellipticals.

Finally we must take into account the uncertainties associated with the difficult measurements of external disk regions of low surface brightness. It is clearly necessary to obtain a larger dataset of absorption spectral indices in spiral disks for galaxies with strong radial gradients of nebular abundances.

4. Discussion: the possible evolutionary histories

The impact of radial distributions of spectral indices on the model predictions can be explained through the effect of the star formation histories on the average stellar abundances. The star formation histories of our 19 models are different and this must imply different mean ages for the stellar populations along galactocentric radius.

This may be clearly seen in Fig. 5 where we represent the star formation history for a inner ($R = 2$ kpc) and a outer ($R = 14$ kpc) disk regions *versus* the oxygen abundance for two models. We have selected for comparison Models 129 and 450, which we consider clearly separated in the input parameter space. The first one is represented by the solid line while the dotted line shows results for the second one. The inner regions have triangles as symbols, and the outer squares. We see that Model 129 is above Model 450 for both regions. Although the final results are not very different, the evolutionary histories truly are, mostly in the inner regions. Therefore mean ages and abundances produced by these models must differ, and, as a result, the spectral indices must be different.

We have computed these averaged ages and abundances for these two regions of the 19 models from Table 1. We represent our results in Fig. 6, panel a) for $R = 2$ kpc and panel b) for $R = 14$ kpc.

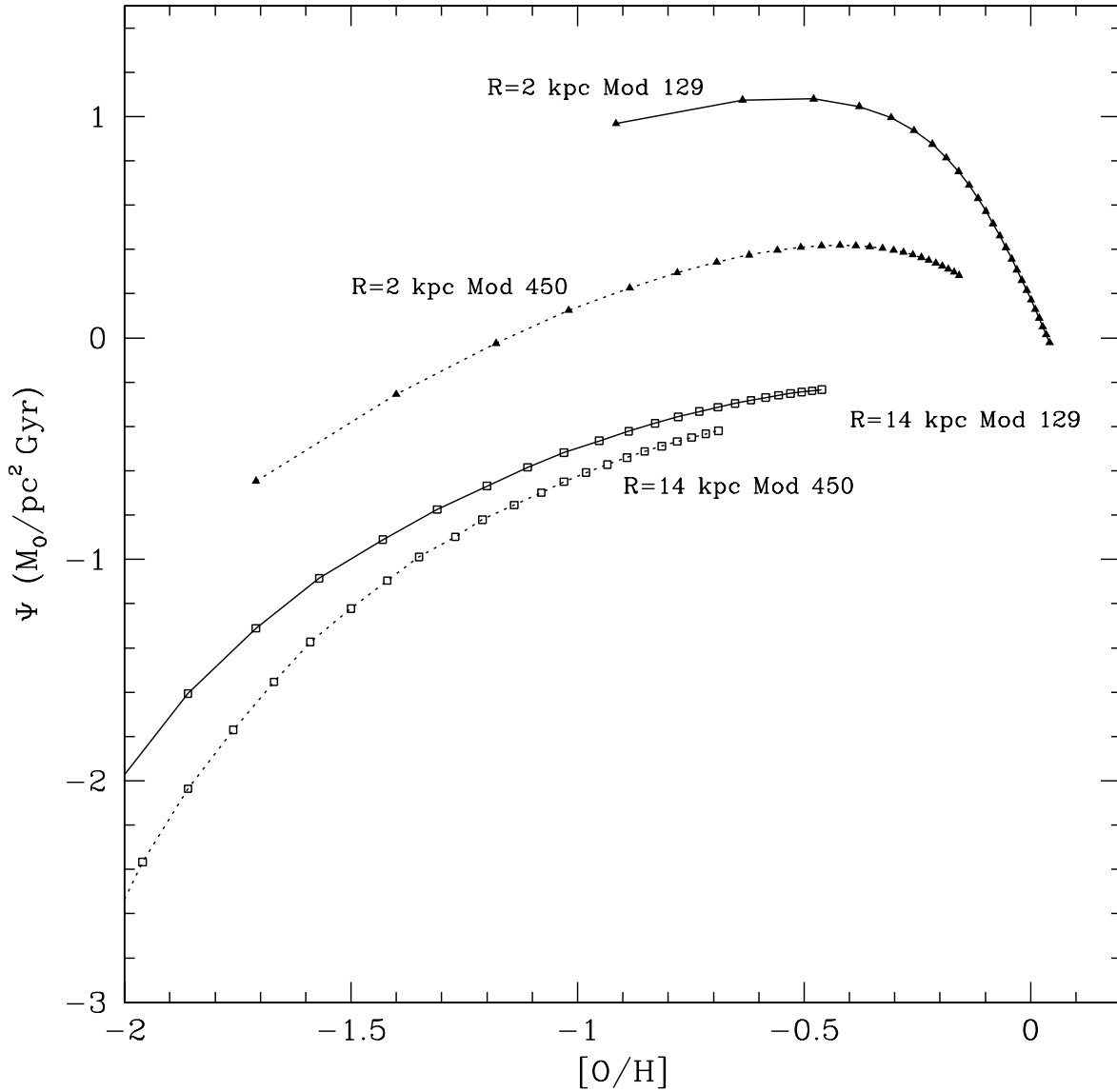


Fig. 5.— Evolution of the star formation rate Ψ vs the oxygen abundance for the inner ($R = 2$ kpc, \triangle symbol) and outer ($R = 14$ kpc, \square symbol) regions for Models 129 (solid lines) and 450 (dotted lines).

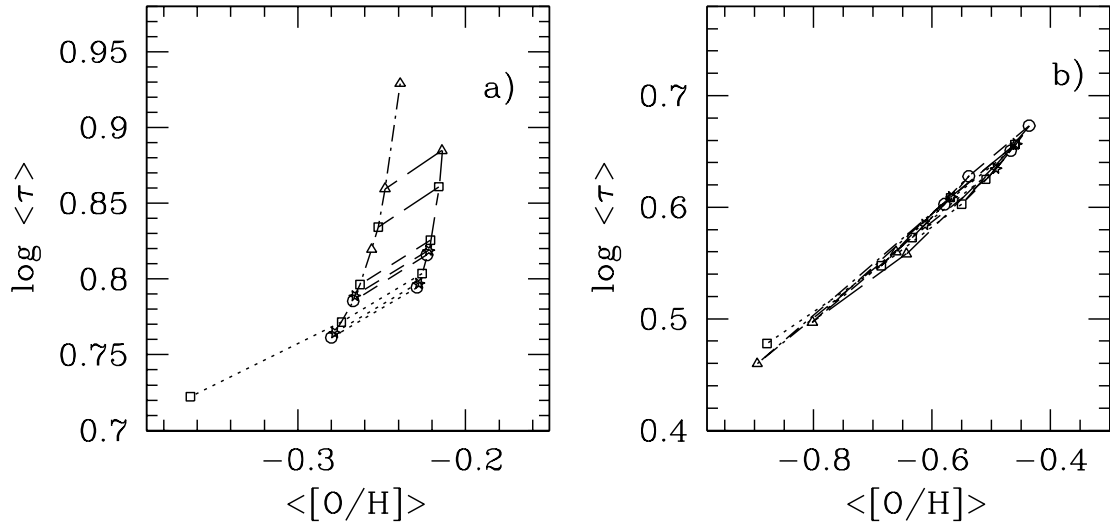


Fig. 6.— The corresponding averaged age of the stellar populations vs the averaged oxygen abundance $\langle [O/H] \rangle$ for the 19 models in 2 radial regions: a) $R=2$ kpc and b) $R=14$ kpc. The two vertical lines in panel a) join models with $T = 4$ (dot-long dashed line) and $T = 4.5$ (short-long dashed line). The square at the left , Model 450, is $T = 5$. Horizontal lines represent $\tau_0 = 8$ (long-dashed line), 12 (short-dashed) and 16 Gyr (dotted line), respectively. The top square is $\tau_0 = 4$ Gyr. Symbols mark different $= \lambda_d$: \triangle for $\lambda_d = 4$; \square for $\lambda_d = 8$; \bullet for $\lambda_d = 12$ and \star for $\lambda_d = 16$ kpc, respectively. Panel b) Symbols have the same meaning than in Panel a).

In panel a), with a point for each model, we see an almost orthogonal diagram. The near-horizontal lines join models with a same collapse time scale, with different symbol following the scale length value (\triangle for $\lambda_D = 4$; \square for $\lambda_D = 8$; \bullet for $\lambda_D = 12$ and \star for $\lambda_D = 15$), while the vertical lines correspond to different efficiencies or T's. Spectral indices depend on both the abundances and the mean ages of the stars which produce them, and we see that Model 129, located at the top of the panel as a triangle, is older and more metal-rich than Model 450, the square located at the left of the same panel. The corresponding spectral indices can not be equal. The other models are located in intermediate positions. The situation for outer regions ($R = 14$ kpc) is shown in panel b) where all models fall in a line.

We can see, however, that for both panels the larger the mean abundances the older the stellar population. This means that the degeneracy problem of Mg₂-Fe52 is not at work here because the result goes in the opposite direction. If the abundances turned out lower in a model than in other we would need a mean age older for the first in order to obtain similar spectral indices, while in fact our low-metal rich models turned out to be the youngest ones. Spectral indices, specially the Mg₂ index, which has a strong dependence on mean age and has a better measurement, will probably discriminate among models better than the gas abundances. This effect is stronger in the outer regions of the disk, as we show in panel b), implying that spectral indices radial distributions may be similar in the inner regions but not in the external ones, where the gas distributions may diverge. This explains the effect shown in Fig. 4.

The star formation histories have two effects on spiral disks: a radial gradient of abundances and a variable mean age for the stellar populations created in each radial region. Thus, even if the radial gradient of abundances obtained from different models are close enough to prevent adequate discrimination, a radial gradient of ages may still exist. Since spectral indices have a dependence on age and on abundances, a radial gradient in the mean ages of the stellar populations implies that radial distributions of indices for different models must differ more than those of abundances, thus helping in selecting the most adequate model or, at least, determining if some of these fall out of the confidence region of the plane defined by the data and their error bars.

5. Conclusions

We have discussed some chemical evolution models and their comparison with data. A first type of models, based purely on the multiphase chemical evolution models that yields direct nebular abundances were constrained by the radial distributions of both atomic and molecular gas. These observational data for the present time (Fig. 2), may be reproduced by only 19 among 500 initial models. Put differently, there are some restricted sets of physically plausible input parameters that provide a superior fit to the abundance data.

Next we computed the spectral index values predicted by the same models through the use of evolutionary synthesis models. These computations rely on a synthesis procedure capable of

establishing the abundance-index relation and which is implemented via the application of the first category of models above. This second category of models, which depends on the first one, may further constrain the chemical evolution of spiral disks by introducing measurements of their stellar content via the determination of spectral absorption indices, such as the Mg₂ and Fe5270 Lick indices. Once again we show that the multiphase model reproduce the generic characteristics of both types of observed radial distributions. The 19 models initially selected on the basis of the nebular data do not reproduced equally well the radial distributions of spectral indices, as can be seen in Table 2: only 5 of them are now good enough to satisfy our criteria.

We also show that statistical differences among models increase when spectral indices radial distributions are used with respect to those using only the present-day oxygen abundances. This effect appears because, even if the present abundances are similar for different models, the averages abundances and ages of the stellar populations responsible for the corresponding spectral indices are not. In fact, in a diagram abundance-age, our results go in the opposite direction than expected from the age-degeneracy problem.

Therefore, by taking into account the results of Table 2, we demonstrate that spectral indices used as time constraints on the evolution of the galaxy are strong enough to eliminate a significant fraction of the models, or to help in the selection of possible scenarios, and we suggest that the measurement of spectral indices must be considered of importance in designing observational projects dealing with the structure of spiral disks.

We thank Dr. A.I. Díaz for useful suggestions. This work has been partially supported by DGICYT project AYA-2000-093. M.Mollá acknowledges the Spanish *Ministerio de Educación y Cultura* for its support through a post-doctoral contract. This work has been use of the Nasa Astrophysics Data System, and the NASA/IPAC Extragalactic Database(NED), which is operated by the Jet Propulsion Laboratory, Caltech, under contract with the National Aeronautics and Space Administration.

REFERENCES

Barbuy, B. 1994, ApJ, 430, 218
Branch, D., & Nomoto, K. 1986, A&A, 164, L13
Beauchamp, D. 1997, *Ph D Thesis*, Université Laval, (Canadá)
Beauchamp, D., & Hardy, E. 1997, AJ, 113, 1666 (Paper I)
Borges, A.C., Idiart, T.P., de Freitas Pacheco, J.A., & Thevenin, F. 1995, AJ, 110, 2408
Buzzoni, A., Gariboldi, G., & Mantegazza, L. 1992, AJ, 103, 1814

Buzzoni, A., Mantegazza, L., & Gariboldi, G. 1994, AJ, 107, 513

Cayatte, V., van Gorkom, J. H., Balkowski, C., & Kotanyi, C. 1990, AJ, 100, 604

Chincarini, G., & de Souza, R. 1985, A&A, 153, 218

Delisle, S. 1998, *Ph D Thesis*, Université Laval,(Canadá)

Díaz A. I. 1989, in Evolutionary Phenomena in Galaxies, eds. J. E. Beckmann & B. E. J. Pagel,(Cambridge: Cambridge University Press), p.377

Distefano, A., Rampazzo, R., Chincarini, G., & de Souza, R. 1990, A&AS, 86, 7

Edmunds, M. G., & Roy, J.-R. 1993, MNRAS, 261, L17

Ferrini, F. & Galli, D. 1988, A&A, 195, 27

Ferrini, F., Matteucci, F., Pardi, C., & Penco, U. 1992, ApJ, 387, 138

Ferrini, F., Mollá, M., Pardi, C., & Díaz, A. I. 1994, ApJ, 427, 745 (FMPD)

Ferrini, F., Mollá, M., & Díaz, A. I. 1997, ApJ, 487, L29

Ferrini, F., Palla F., & Penco, U. 1990, A&A, 213, 3

de Freitas-Pacheco, J. A. 1998, in Abundances Profiles:Diagnostic Tools for Galaxy History, Eds. D. Friedli, M. G. Edmunds,C. Robert, & L. Drissen, ASP Conference Series, p. 205

Gallagher, J. S., Hunter, D. A., & Tutukov, A. V. 1984, ApJ, 284, 544

Garnett, D. R., Shields, G. A., Skillman, E. D., Sagan, S. P., & Dufour, R. J. 1997, ApJ, 489, 63

Götz, M., & Köppen, J. 1992, A&A, 262, 455

Guhathakurta, P., van Gorkom, J. H., Kotanyi, C. C., & Balkowski, C. 1988, AJ, 96, 851

Henry, R. B. C. 1993, MNRAS, 261, 306

Henry, R. B. C., Pagel, B. E. J., Lassiter, D .F., & Chincarini, G. 1992, MNRAS, 258, 321

Henry, R. B .C., Balkowski, C., Cayatte, V., Edmunds, M. G. & Pagel, B. E. J. 1996, MNRAS, 283, 635

Kennicutt, R. C.,Jr. 1989, ApJ, 344, 685

Kennicutt, R. C., Jr. & Garnett, D.R. 1996, ApJ, 456, 518

Kenney, J. D., & Young, J. S. 1988, ApJ, 326, 595

Kenney, J. D., & Young, J. S. 1989, ApJ, 344, 171

Köppen, J. 1994, A&A, 281, 26

Martin, P., & Roy, J.- R. 1992, ApJ, 397, 476

Martin, P., & Roy, J.- R. 1994, ApJ, 424, 599

Martin, P., & Roy, J .R 1995, ApJ, 445, 161

McCall, M. L., Rybsky, P. M., & Shields, G. A. 1985, ApJSS, 57, 1

Mollá, M., Díaz, A. I., & Ferrini, F. 1992, in The feedback of Chemical Evolution on the Stellar Content of Galaxies,Eds. D. Alloin & G. Stasinska (Observatoire de Meudon, Paris), p. 258.

Mollá, M., Díaz, A. I., & Ferrini, F. 2001, in preparation

Mollá, M., Ferrini, F., 1995, ApJ, 454,726

Mollá, M., Ferrini, F., & Díaz, A. I. 1996, ApJ, 466, 668

Mollá, M., Ferrini, F., & Díaz, A. I. 1997, ApJ, 475, 519

Mollá, M., Hardy, E., & Beauchamp, D. 1999, ApJ, 513, 695 (Paper II)

Mollá, M., Ferrini, F., & Gozzi, G. 2000, MNRAS, 316, 345.

Mollá, M. & García-Vargas, M.L. 2000, A&A, 359, 18

Nomoto, K., Thielemann, F. K., & Yokoi, K. 1984, ApJ, 286, 644

Pilyugin, L.S. & Ferrini, F. 1998, A&A, 336, 103

Pilyugin, L. S. 2000, A&A, 362, 325

Renzini, A., & Voli, M. 1981, A&A, 94, 175

Shields, G. A., Skillman, E. D., & Kennicutt, R .C. 1991, ApJ, 371, 82

Skillman, E. D., Kennicutt, R. C., Shields, G. A., & Zaritsky, D. 1996, ApJ, 462, 147

Taylor, C. L. & Klein, U. 2001, A&A, 366, 811

Thomas, D. 2001, Astrophysics & Space Science Suplement, 277, 209

Tinsley, B.M 1980, Fund. Cosmic. Phys., 5, 287

Tosi, M., 1988, A&A, 197, 33

Tosi, M. 1996, in From Stars to Galaxies: the impact of stellar physics on galaxy evolution, PASP Conference Series,vol 98, Eds. C. Leitherer, U. Fritze-von Alvensleben, & J. Huchra, p.299

Verter, F, & Hodge, P. 1995, ApJ, 446, 616

Warmels, R. H. 1988, A&AS, 72, 427

Wilson, C. D. 1995, ApJ, 448, L97

Woosley , S. E., & Weaver, T. A. 1995, ApJS, 101, 181

Worthey, G. 1994, ApJS, 95, 107

Worthey, G., Faber, S. M., González, J. J., & Burstein, D. 1994, ApJSS, 94, 687